AFRL-AFOSR-VA-TR-2020-0049

The effects of strong wall cooling on supersonic and hypersonic shock/boundary-layer interactions

Johan Larsson
MARYLAND UNIV COLLEGE PARK

12/06/2019
Final Report

Air Force Research Laboratory
AF Office Of Scientific Research (AFOSR)/ RTA1
Arlington, Virginia 22203
Air Force Materiel Command

REPORT DOCUMENTATION PAGE

Form Approved
OMB No. 0704-0188

1. REPORT DATE *(DD-MM-YYYY)*	2. REPORT TYPE	3. DATES COVERED *(From - To)*
05-06-2020	Final Performance	15 Sep 2016 to 31 Aug 2019

4. TITLE AND SUBTITLE
The effects of strong wall cooling on supersonic and hypersonic shock/boundary-layer interactions

5a. CONTRACT NUMBER

5b. GRANT NUMBER
FA9550-16-1-0385

5c. PROGRAM ELEMENT NUMBER
61102F

6. AUTHOR(S)
Johan Larsson, Tamer Zaki

5d. PROJECT NUMBER

5e. TASK NUMBER

5f. WORK UNIT NUMBER

7. PERFORMING ORGANIZATION NAME(S) AND ADDRESS(ES)
MARYLAND UNIV COLLEGE PARK
3112 LEE BLDG
COLLEGE PARK, MD 20742 - 5100 US

8. PERFORMING ORGANIZATION REPORT NUMBER

9. SPONSORING/MONITORING AGENCY NAME(S) AND ADDRESS(ES)
AF Office of Scientific Research
875 N. Randolph St. Room 3112
Arlington, VA 22203

10. SPONSOR/MONITOR'S ACRONYM(S)
AFRL/AFOSR RTA1

11. SPONSOR/MONITOR'S REPORT NUMBER(S)
AFRL-AFOSR-VA-TR-2020-0049

12. DISTRIBUTION/AVAILABILITY STATEMENT
A DISTRIBUTION UNLIMITED: PB Public Release

13. SUPPLEMENTARY NOTES

14. ABSTRACT
We completed all 3 phases of the project. The first phase (Mach 2.3 study) was published in Phys. Rev. Fluids in 2018. The second phase (helping DLR design their Mach 7.4 experiment) was completed primarily during the second year and presented at the 2019 AIAA Scitech meeting. This experiment will now be conducted at DLR during 2020. The final phase of this project was to extend the DNS study to the hypersonic regime in order to understand how the effect of wall-cooling changes with Mach number. This was done by performing DNS of an existing Mach 5.0 experiment from DLR, which confirmed some findings from the Mach 2.3 study but also showed significant differences in the scaling of the interaction length. These findings are currently under review for the Phys. Rev. Fluids journal.

15. SUBJECT TERMS
Van Driest transformation, wall cooling shock boundary layer, hypersonic shock boundary layer interactions, hypersonics

16. SECURITY CLASSIFICATION OF:			17. LIMITATION OF ABSTRACT	18. NUMBER OF PAGES	19a. NAME OF RESPONSIBLE PERSON
a. REPORT	b. ABSTRACT	c. THIS PAGE			LEYVA, IVETT
Unclassified	Unclassified	Unclassified	UU		19b. TELEPHONE NUMBER *(Include area code)* 703-696-8478

Standard Form 298 (Rev. 8/98)
Prescribed by ANSI Std. Z39.18

The effects of strong wall cooling on supersonic and hypersonic shock/boundary-layer interactions

FA9550-16-1-0385

Johan Larsson
Department of Mechanical Engineering, University of Maryland, College Park
E-mail: jola@umd.edu; Phone: 301-405-5273

Final Report,
submitted to Dr. Ivett Leyva on November 26, 2019.

Summary

Shock/boundary-layer interactions (SBLI) are important in many high-speed flight applications, and as such have been studied in great detail in many past scientific studies. The core premise of this work is the following dichotomy: while the thermal condition of the wall may vary from adiabatic to strongly cooled in many important Air Force applications, the vast majority of prior scientific SBLI studies have either studied the canonical case of an adiabatic wall or, in cases where the wall was non-adiabatic, have not systematically varied this parameter in order to isolate the effects of wall-cooling.

The objective of this project is to fill this gap by conducting a sequence of direct numerical simulations (DNS) for geometrically simple SBLI problems where the wall temperature (T_w) and the shock strength are systematically varied. The work originally had the following partially overlapping phases:

1. Isolating the hydrodynamic effect of wall-cooling by studying a supersonic (ideal gas) case at Mach 2.3 (with reference data from an existing experiment at Marseille);
2. Working with our partners at DLR to design a new validation experiment in the hypersonic regime (Mach 7.4) with systematically varied wall-temperature; and
3. Studying the combined hydrodynamic and thermo-chemistry effects of wall-cooling by simulating (using DNS) the Mach 7.4 DLR experiment.

Phase 1 was completed around the mid-point of Year 2 and has since been published in *Phys. Rev. Fluids* [1]. Phase 2, helping Alexander Wagner at DLR design the new Mach 7.4 experiment, was completed (our component of it) during Year 2. We performed LES runs at different shock strengths (i.e., angles) to estimate the size of the separation bubble, which has since been used by Alexander Wagner to choose the specific shock strengths in the experiment (large enough to be measured; small enough to avoid spanwise edge effects; located at the region of the plate with surface measurement access; etc). This "experimental-design" study was presented at the 2019 AIAA SciTech meeting, as a collaboration between UMD and DLR [2].

The actual experiment at DLR was delayed and will now be conducted during 2020. We therefore modified Phase 3 of this project to instead study (using DNS) a Mach 5.0 SBLI problem which was studied experimentally by Schülein [3]. This accomplishes the same goal as the original plan: to test all findings from Mach 2.3 at a higher Mach number. The findings of this study are currently under review for publication in the *Phys. Rev. Fluids* journal [4].

1 Mach 2.3 study

This study uses DNS to study the shock/boundary-layer interaction corresponding to the experiment by Jaunet *et al.* [5], in which a Mach 2.3 boundary layer is impinged upon by an oblique shock generated by a wedge in the free stream. This experimental set-up is very common, but the unique aspect of this study (and some prior studies in the same lab at Marseille) is that they measured the same flow with an adiabatic wall and a uniformly heated wall. Quantifying the degree of wall cooling/heating by the wall-to-recovery temperature ratio, they performed experiments at $T_w/T_r = 1.0$ (adiabatic) and $T_w/T_r = 1.9$ (heated).

Sample results are shown in Fig. 1. The main point is the dramatic effect of the imposed wall temperature, with a much smaller interaction region for lower T_w.

We performed about 12 simulations of this SBLI problem during Year 1 of the project, with three different temperature ratios (the ones from the experiment plus a cooled case with $T_w/T_r = 0.5$). During the second year of the project, we completed an additional 5-10 simulations, aimed at: (i) expanding the number of shock strengths (flow deflection angles) covered; (ii) verifying grid convergence; (iii) assessing the Reynolds number effects by computing one case at a higher Reynolds number; and (iv) testing with spatially non-uniform T_w profiles.

The full details are given in the journal paper [1], and we give only the main conclusions here.

The semi-empirical scaling of the interaction length (effectively, the size of the separation bubble) proposed by Jaunet *et al.* [5] was found to describe the present DNS results well. The additional simulations at smaller and higher flow deflection angles meant that our DNS data covers the full range of the experimental conditions obtained in the experiment. The one caveat here is that all of the experimental data used to test the Jaunet *et al.* scaling to date has been from Mach 2-3, meaning that the theory really needs to be tested at larger Mach numbers. This is the reason for focusing on a higher Mach number case in the final phase of the project.

The simulation at the higher Reynolds number improved the agreement between the current DNS and the experimental data by Jaunet *et al.*, thus providing confidence that the minor, very systematic, disagreement between the current DNS and the experimental data is most likely due to the differences in the Reynolds number.

An interesting test was to make the wall temperature T_w non-constant in the streamwise direction. Specifically, it was set to the adiabatic value ($T_w/T_r = 1$) in the incoming boundary layer and switched to the heated value ($T_w/T_r = 1.9$) immediately before the interaction; we also tried the opposite combination. The results of these cases were then compared to the cases with uniform T_w. The adiabatic-to-heated case agreed quite well with the adiabatic-everywhere case, while the heated-to-adiabatic case produced a result somewhere between the uniformly heated and uniformly adiabatic. Our conclusion is, therefore, that the effect of the wall temperature is not purely local. This has a direct implication to the possibility of using tailored cooling patterns to control a flow (e.g., in an isolator): the present results show that it is not sufficient to have a cold wall immediately under the SBLI, but one should cool the wall some distance upstream as well. From a more scientific point-of-view, this result shows that the "pathway" for how the wall thermal condition affects the flow is at least partly through the incoming boundary layer (where cooling produces a more full velocity profile).

A surprising finding was that wall cooling produces a higher peak p'_{rms} in the interaction zone, as shown in Fig. 2. Our expectation had been that since cooling reduces the size of the interaction region and to some degree stabilizes it, it would also produce lower pressure fluctuations; we were associating pressure fluctuations with the stability and size of the interaction. The results, however, were the opposite. In hindsight, the most plausible explanation is that wall cooling produces a sharper pressure rise (in x) which, when coupled with the oscillating shock, produces a larger

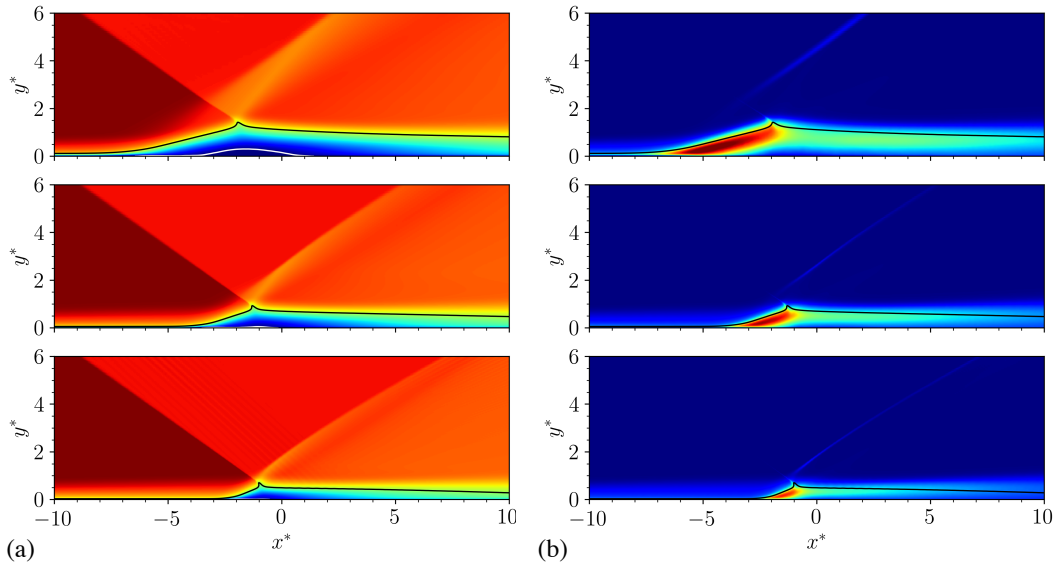

Figure 1: Mean streamwise velocity (left) and turbulence kinetic energy (right) at $T_w/T_r = 1.9$ (heated wall; top), $T_w/T_r = 1.0$ (adiabatic wall; middle), and $T_w/T_r = 0.5$ (cooled wall; bottom). All cases are at Mach 2.3 with the same flow deflection angle (i.e., identical shock strengths). From [1].

pressure fluctuation. From an applied perspective, this result suggests that there are drawbacks to using wall cooling to stabilize shock/boundary-layer interactions, specifically the potential for larger structural loads.

2 Helping DLR design the Mach 7.4 experiment

In a separate project, Alexander Wagner at DLR will perform an experiment of a shock/boundary-layer interaction aimed at providing validatation data on the effect of changing the wall temperature. After discussions, this experiment will be performed at Mach 7.4 with an incoming boundary layer that develops over a flat plate that is kept at either $T_w = 300$K or $T_w = 800$K, corresponding to $T_w/T_r = 0.13$ (very strongly cooled) and $T_w/T_r = 0.33$ (less strongly cooled). We debated between a compression ramp geometry and an impinging shock geometry. After discussions, the decision was made to pursue the impinging shock geometry.

An important design issue is to ensure a fully developed turbulent boundary layer. This will require significant tripping of the boundary layer; with a more "natural" transition process, the boundary layer does not fully transition before the interaction region. The design of the trip is handled by Alexander Wagner.

The other important design parameter is which flow deflection angle(s) to perform experiments at. We want interactions that are sufficiently large in size to enable meaningful measurements, and also interactions that have comparable scaled interaction sizes as those at Mach 2.3 in order to make comparisons and test the Jaunet *et al.* [5] scaling. To support this decision, we performed LES of this flow at both wall temperatures, for 3 different flow deflections, during Year 2 and parts of Year 3 of the project. The simulations are summarized in Table 1.

Our computational work was presented at the AIAA SciTech meeting in January 2019 [2].

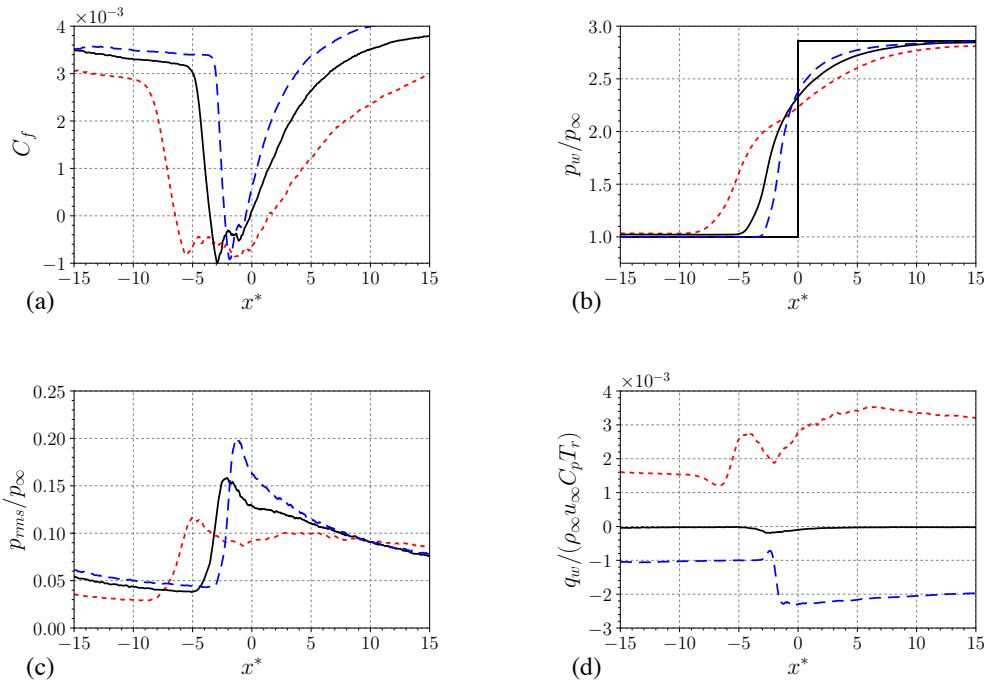

Figure 2: Results from Mach 2.3 and identical shock strengths, for $T_w/T_r = 1.9$ (heated wall; red dashed), $T_w/T_r = 1.0$ (adiabatic wall; black solid), and $T_w/T_r = 0.5$ (cooled wall; blue long-dashed). From [1].

Simulation	T_w/T_r	φ	T_w/T_∞	Grid points	L_{sep}/δ_0
SBLI-0.33-12	0.33	12°	2.77	45 M	1.2
SBLI-0.33-15	0.33	15°	2.77	45 M	3.3
SBLI-0.33-18	0.33	18°	2.77	45 M	5.5
SBLI-0.13-12	0.13	12°	1.12	109 M	0.6
SBLI-0.13-15	0.13	15°	1.12	109 M	1.8
SBLI-0.13-18	0.13	18°	1.12	109 M	3.9

Table 1: Summary of LES at Mach 7.4 performed to support design of the DLR experiment. Taken from [2].

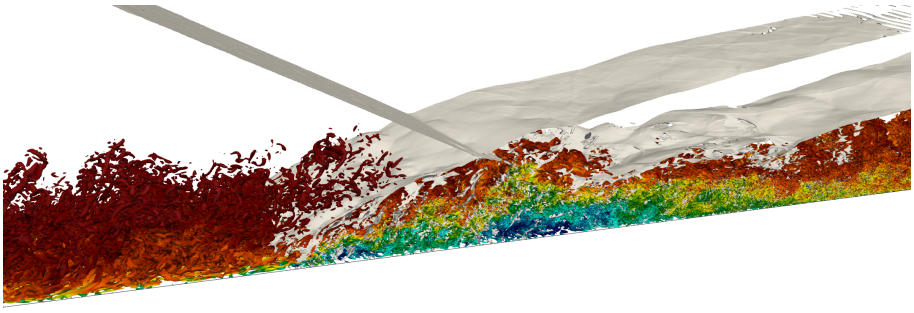

Figure 3: Visualization of the Mach 5.0 SBLI at $T_w/T_r = 0.8$ and the strongest incoming shock.

3 Mach 5.0 study

The planned Mach 7.4 experiment at DLR was delayed and will now be performed during 2020. Recognizing the need for tests at higher Mach numbers in the present study, we therefore chose to perform simulations of a Mach 5.0 experiment performed by Schülein [3] in a different facility at DLR. This is a low-enthalpy case ($T_0 = 410$K) but has a substantially higher Mach number than our previous computations. The experiment was performed with a fixed nearly adiabatic wall with $T_w/T_r = 0.8$, and with 3 different shock generators with flow deflection angles of 6°, 10°, and 14°. Skin friction was measured by an oil flow technique and also computed indirectly from log-law curve fits to the measured velocity. Heat transfer was measured by infrared thermography.

Simulations were performed at the experimental $T_w/T_r = 0.8$ and an additional $T_w/T_r = 1.9$, where the latter was chosen partly for comparisons with our prior work at Mach 2.3 and partly since this is close to the largest temperature ratio that could be achieved easily in this facility (prior DLR experiments have used up to $T_w \approx 800$ K). Simulations were performed at 3 different Reynolds numbers to assess the sensitivity of the results. In the following, coordinates are made non-dimensional by the boundary layer thickness δ_{imp} at the inviscid shock impingement point x_{imp}.

3.1 Effect of deflection angle and comparison with experiments

As described by Delery and Dussauge [6], there are two shock waves in a weak SBLI: the impinging shock and the reflected shock formed by the compression waves coming from the front and rear portion of the expanded boundary layer subsonic region. In this case, the pressure rises smoothly through the interaction region attaining the inviscid pressure jump. In a strong interaction, on the other hand, the boundary layer detaches and the mean pressure profile through the interaction region exhibits a plateau in the separation zone. At the leading edge of the separation bubble, compression waves form the reflected shock. The flow deflection at the top of the bubble generates an expansion fan followed by compression waves that may or may not gather with the compression wave generated at the leading edge of the separation bubble (see Figs. 3 and 4).

Here, we study configurations characteristic of weak, incipient and strong interactions. Differently from supersonic SBLI studies, the strong interaction ($\varphi = 14°$) presents two strong reflected waves as illustrated in Fig. 3, which shows the three-dimensional field of the Q-criterion iso-surface colored by the streamwise velocity and dilatation iso-surface to illustrate incident and reflecting shocks. This 3D visualization highlights the turbulent structures of the boundary layer and the complex waves that are originated by the interaction.

Figure 4 shows the instantaneous and mean streamwise velocity fields in the xy plane for cases

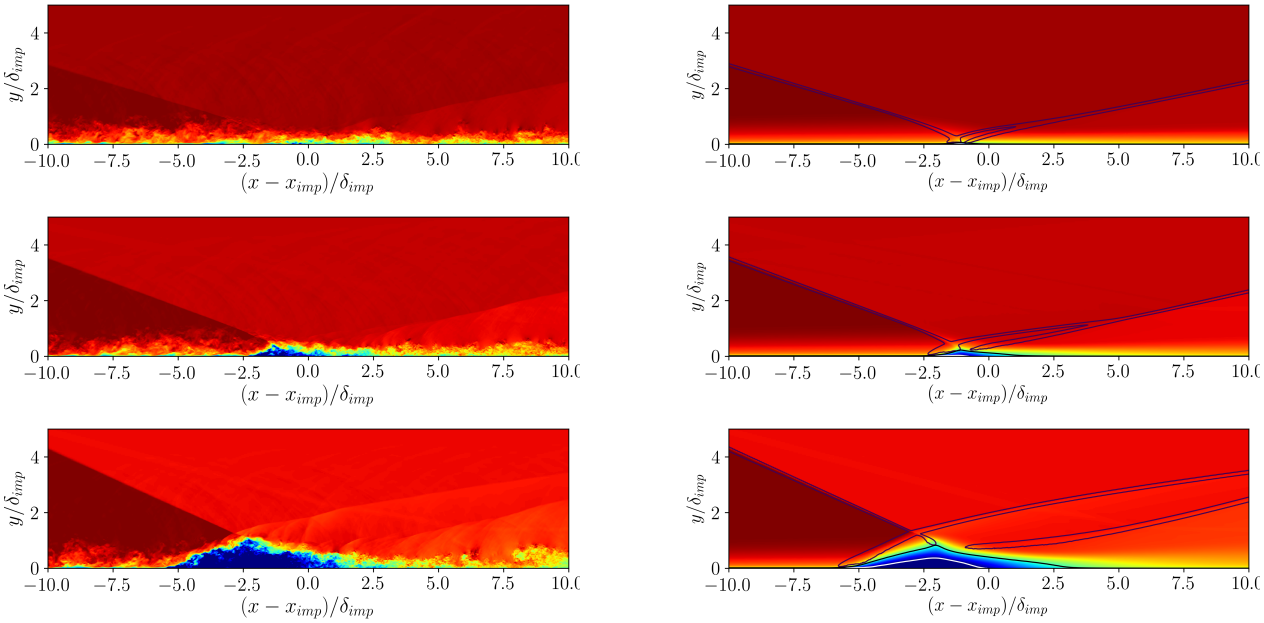

Figure 4: Instantaneous (left) and mean (right) streamwise velocity field $\overline{u}$ at various incidence angle of the shock generator and $T_w/Tr = 0.8$: $\varphi = 6°$ (case SBLI-0.8-06), $\varphi = 10°$ (case SBLI-0.8-10) and $\varphi = 14°$ (case SBLI-0.8-14) from top to bottom. Contour levels are shown in the range $0 < \overline{u}/u_\infty < 1$. The white line denotes the zero level and the black one the sonic line. Iso-contour of the mean dilatation is also shown in dark purple.

with $\varphi = 6°$, $10°$ and $14°$. It is clear that the size of the recirculation bubble increases when φ increases.

Simulations with $T_w/T_r = 0.8$ are now analyzed and compared with experimental data. The average skin friction coefficient $C_f = 2\tau_w/\rho_\infty u_\infty^2$ is displayed in Fig. 5(a) for the three deflection angles considered. The friction coefficient is qualitatively different from the $M_\infty = 2.3$ results [1], where C_f became distinctly negative immediately at separation; in the present $M_\infty = 5$ results, C_f instead becomes only slightly negative at first, followed by a later dip.

The experiments by Schulein [3] have qualitatively similar C_f profiles (a weakly negative region followed by a more pronounced dip) but with much earlier separation: the boundary layer separates about $2\delta_{imp}$ earlier for $\varphi = 14°$ and about δ_{imp} earlier for $\varphi = 10°$. For the $\varphi = 6°$ case, the experiment (data not shown in the figure) indicates attached flow without any separation while the DNS has a very small separated region.

The reason for this disagreement is not known. One possible explanation is the boundary layer on the wedge that creates the impinging shock, which would increase the shock strength and also cause an upstream shift of the shock impingement location. However, this hypothesis is rejected here since the mean pressure jumps agree very well between the experiment and the DNS (Fig. 5(b)). Another hypothesis is that the disagreement is a Reynolds number effect. However, the difference between the high and nominal Reynolds number cases in Fig. 6 is very small, and we therefore reject this hypothesis as well. The next possibility is that the disagreement stems from differences in the incoming boundary layer. The skin friction coefficient C_f is slightly smaller in the experiment than in the DNS, but the Stanton number is smaller by almost a factor of two in the experiment. The temperature in the DNS closely follows the Walz relation (not shown) and is fully developed at the shock impingement location. The DNS does not have an entropy layer since we do not include

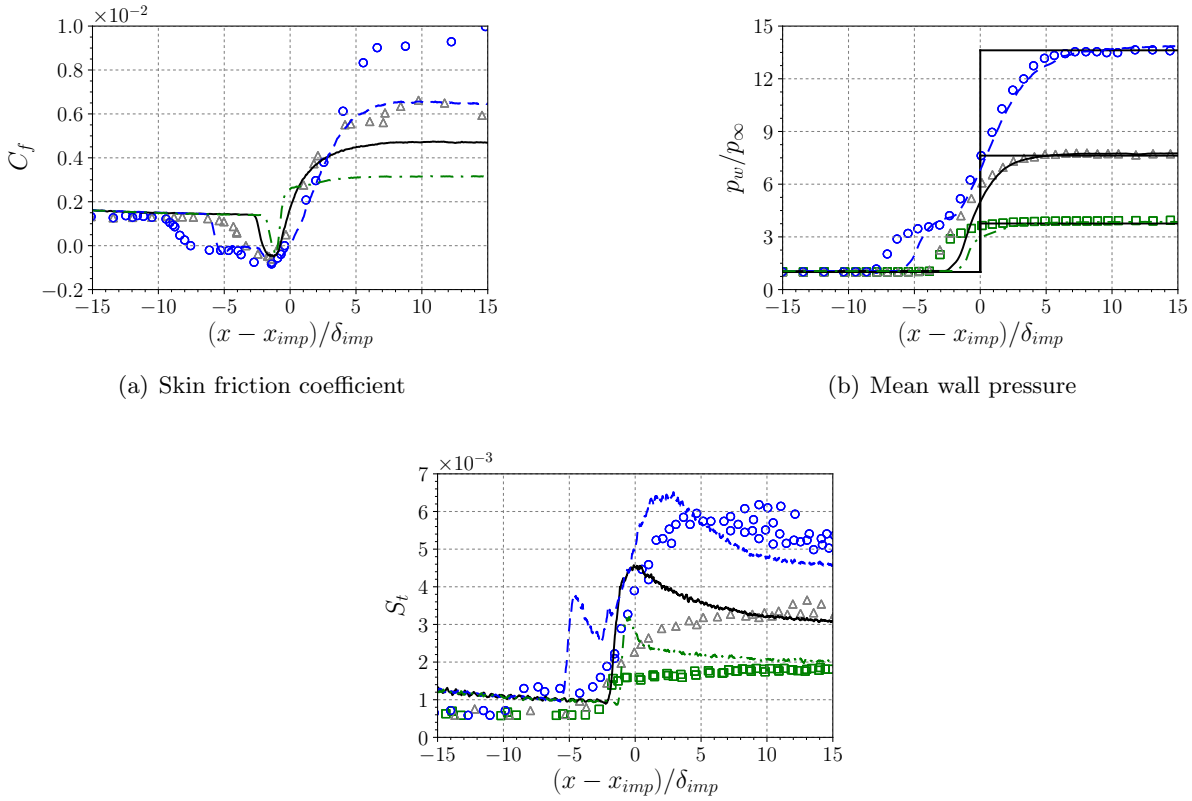

(a) Skin friction coefficient

(b) Mean wall pressure

(c) Mean Stanton number

Figure 5: Mean flow properties across the interaction zone at various deflection angles and $T_w/Tr = 0.8$: case SBLI-0.8-14 (dashed), SBLI-0.8-10 (solid) and SBLI-0.8-06 (dashed-dotted line). Symbols indicate experimental data from Schulein [3].

the leading edge in the computation, but this difference should cause a larger wall heat flux in the experiment, opposite of what is observed; in addition, the experiment was conducted with a very sharp leading edge which should not cause a large entropy layer. The last hypothesis is that the discrepancy is caused by 3D effects, i.e., by the finite span of the plate in the experiment. Bruce *et al.* [7] studied the effect of confinement from tunnel walls (and the associated corner flows) on planar SBLI, and found that the effect could be parametrized by the ratio of the displacement thickness δ^* to the width of the test section. In very approximate terms, they found the effect of confinement to be significant for $\delta^*/L_z \gtrsim 0.002-0.004$. The equivalent parameter for the experiment by Schulein [3] is $\delta^*/L_z \approx 0.005$. While the confinement characteristics of the latter is entirely different (a flat plate without sides immersed in a free stream), it nevertheless seems plausible that the experiment has significant 3D effects. Of particular note is that Bruce *et al.* [7] found a rather strong effect on the size and location of the separation bubble. To conclude, while the reason for the discrepancy between the DNS and the experiment is not known at this point, the most plausible explanation is that the discrepancy is caused by 3D effects, specifically related to the effect of the finite width of the flat plate in the experiment. We note that inclusion of the full width of the plate would increase the computational cost by at the very least a factor of 30.

The mean wall pressure normalized by the free-stream pressure is shown in Fig. 5(b). The pressure jump predicted by the inviscid theory is well recovered in both cases. The mean wall

pressure distribution is typical of a weak interaction for $\varphi = 6$ and 10 deg. and typical of strong interaction for $\varphi = 14$ deg. In the first case, the pressure rise is smooth, while in the latter, a pressure plateau is observed.

The heat transfer rate can be characterized by the spatial distribution of the Stanton number

$$St = \frac{q_w}{\rho_\infty u_\infty C_p (T_w - T_r)}, \quad q_w = -k \left. \frac{d\overline{T}}{dy} \right|_w \tag{1}$$

which is plotted in Fig. 5(c). Note that Schulein [3] used the stagnation temperature T_0 instead of the recovery temperature T_r in the definition of the Stanton number; this was rescaled to use T_r in all plots here. A strong amplification of the heat transfer rate is found in the interaction region with respect to the reference boundary layer and is higher for large shock strengths. For case $\varphi = 14°$, the heat transfer rate is around 7 times higher than the reference boundary layer case before the interaction. The Stanton number distribution has a minimum at the mean separation point and increases non-monotonically for strong interactions.

3.2 Effect of wall temperature on the SBLI flow field

The spatial distribution of the mean skin friction coefficient C_f is shown in Fig. 6(a). The heated case separates first and reattaches practically in the same location as the cooled case. The agreement between numerical and wind-tunnel results is relatively good in the undisturbed boundary layer. In the interaction, curiously, it seems that the heated case compares better with the experiment at the beginning of the interaction. For $(x - x_{imp})/\delta_{imp} > 0$, the agreement is better for the cooled simulation. The skin friction distribution gradually relaxes to that of an equilibrium boundary layer, but in this region the experimental uncertainty is quite large. Note that the simulation at higher Reynolds number SBLI-0.8-14-H does not show a big discrepancy if compared to the one performed at lower Reynolds number. Thus, it appears that the impact of the shock strength or wall cooling is more important than the Reynolds number in determining the size of the interaction length scales.

The spatial distribution of the mean wall pressure p_w for the same cases, as well as the pressure jump predicted by the inviscid theory, are plotted in Fig. 6(b). Both simulations are typical of strong interactions, but the pressure plateau for the cooled case is smaller than the heated one. The final pressure is equal to the inviscid value in both cases. In Fig. 6(b) the plateau pressure prediction by Zukoski [8] is also plotted as reference.

It was found in supersonic SBLI that the peak root-mean-square wall pressure p_{rms} was stronger in cooled cases [9, 1]. At $M_\infty = 2.28$, for example, the peak value for a case with wall conditions $T_w/T_r = 0.5$ was found to be ~ 1.6 times higher than for a case with $T_w/T_r = 1.9$. Figure 6(c) shows that for the present configurations, the maximum values of the wall pressure fluctuation are practically the same in both situations. The wall-pressure fluctuations for simulations with $\varphi = 6°$ (not shown) show only one local maximum, similar to the supersonic SBLI results from the previous study [1]. If the shock strength is very strong, it is possible to obtain two local peaks [10], as in SBLI-0.8-14. This is related to the shock foot location, specifically that the second reflected shock bifurcates (see Fig. 7), generating the middle peak. The mean turbulence kinetic energy $k = \widetilde{u_i'' u_i''}/2$ is amplified in the shear layer and also in the reflected shock location as clearly visualized in Fig. 8. Interestingly, the heated $\varphi = 14°$ case (SBLI-1.9-14) shows a further qualitative change with an extended region of elevated p_{rms} between the point of separation and the first p_{rms} peak.

Figure 6(d) characterizes the heat transfer behavior across the interaction. Here, the heat transfer is normalized by $\rho_\infty u_\infty C_p T_r$ to allow a direct comparison between the heated and cooled cases. A strong amplification of the heat transfer rate is found in the interaction region with respect

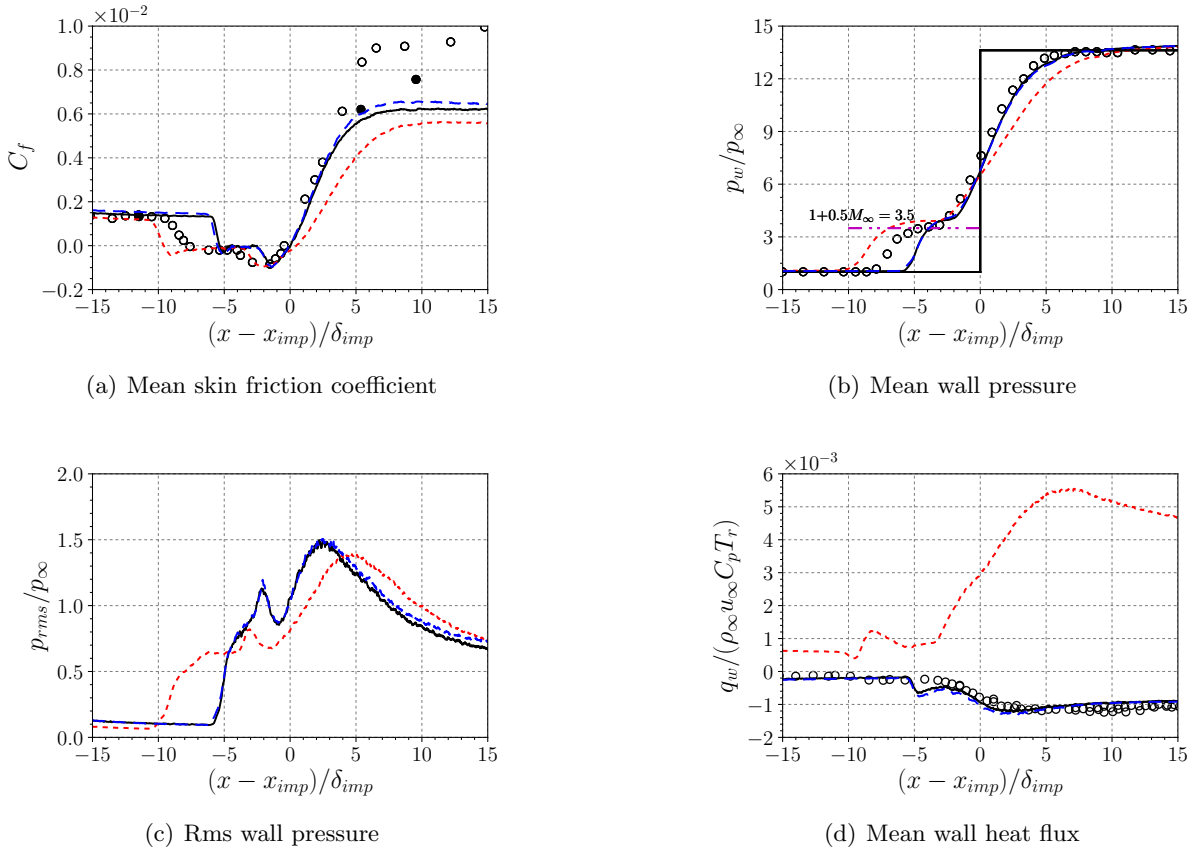

(a) Mean skin friction coefficient

(b) Mean wall pressure

(c) Rms wall pressure

(d) Mean wall heat flux

Figure 6: Mean flow properties across the interaction zone at $\varphi = 14°$ flow deflection: cases SBLI-1.9-14 (dotted), SBLI-0.8-14 (dashed), and SBLI-0.8-14-H (solid). The symbols indicate experimental measurements from Schulein [3]. In (a), the open circles are from oil film interferometry while the closed circles are from the measured velocity profile. The plateau pressure prediction according to Zukoski [8] is also shown in (b).

to the reference cooled or heated boundary layers, with a maximum increase of approximately a factor of 7 for the cooled wall and 9 for the heated wall. Note that these values are much higher than in the supersonic cases.

A useful correlation of heating variation with pressure for shock/turbulent boundary layer interaction was found by Back and Cuffel [11]. They stated that the heat flux (or Stanton number) should scale as

$$\frac{q_{w,max}}{q_{w,0}} = \left(\frac{p_{max}}{p_\infty}\right)^n \tag{2}$$

where p_{max}/p_∞ is the inviscid surface pressure ratio across the shock wave, $q_{w,0}$ is the wall heat flux value calculated in the incoming boundary layer, here taken at $x_0 = 21\delta_{in}$. Back and Cuffel [11] and Holden [12] found $n = 0.85$ experimentally, while Hung and Barnett [13] obtained $n = 0.80$. Figure 9 shows the correlation of maximum heating with shock strength. Also plotted in the graphic are the laws that best describe the trend. While $n = 0.85$ describes precisely the trend for SBLI with a heated wall, for SBLI with cooled walls n is found to be relatively lower at the present conditions. We also note that the peak Stanton number occurs in the region where we found the largest uncertainties in the present results during the solution verification, and thus these results

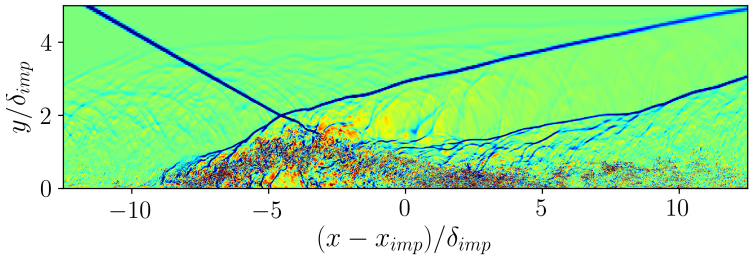

Figure 7: Instantaneous dilatation field $\xi = \partial_j u_j$ for simulation with $T_w/T_r = 1.9$ and $\varphi = 14°$ (case SBLI-1.9-14). Contour levels are shown in the range $-1 < \xi < 1$.

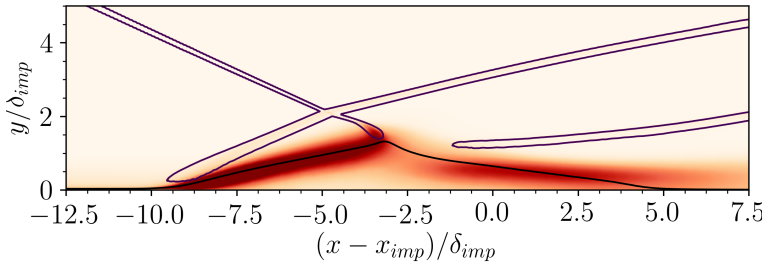

Figure 8: Mean turbulence kinetic energy $k = \widetilde{u_i'' u_i''}/2$. Contour levels are shown in the range $0 < k/u_\infty^2 < 0.04$ with $T_w/T_r = 1.9$ and $\varphi = 14°$(case SBLI-1.9-14). The black line denotes the sonic line. Iso-contour of the mean dilatation is shown in dark purple.

should be taken as approximate.

3.3 The free interaction theory

Once a boundary layer separates, the flow field in the region near separation is dominated by the equilibrium interaction between the boundary layer and the external flow. Although the location of the point of separation is a function of the location and strength of the disturbance, the interacting flow upstream of the separation depends neither on the source of separation nor on the downstream geometry. This observation led Chapman *et al.* [14] to formulate the "free interaction" theory. A detailed description of the free interaction theory can be found in Refs [15, 16, 17, 18, 19].

It can be shown that the non-dimensional similarity variables within the free interaction zone are given by

$$\mathcal{P} = \frac{p - p_0}{q_0} \left[\frac{(M_0^2 - 1)^{1/2}}{2C_{f0}} \right]^{1/2} \tag{3}$$

$$\mathcal{X} = \frac{x - x_{sep}}{\delta_0^*} \left[(M_0^2 - 1)^{1/2} C_{f0} \right]^{1/2} \tag{4}$$

where $q_0 = 0.5\rho_0 u_0^2$. The subscript 0 indicates a reference point near beginning of separation interaction, taken as $x_0 = 21\delta_{in}$. The similarity function $\mathcal{P}(\mathcal{X})$ is plotted in Fig. 10.

It is remarkable how the initial pressure rise is almost identical among all present cases, including heated/cooled and different shock angles producing both weak and strong interactions. When comparing with other studies, however, the $\mathcal{P}(\mathcal{X})$ function does not appear to be universal. Defining $\mathcal{P}_s$ to be the value at the point of separation (i.e., at $\mathcal{X} = 0$), the present cases all have $\mathcal{P}_s \approx 1$.

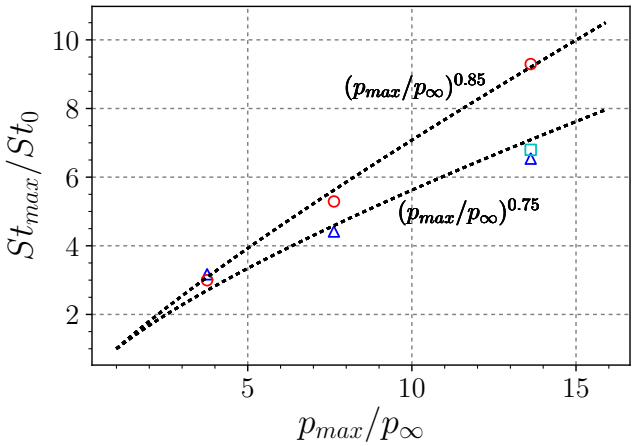

Figure 9: Correlation of maximum heating with shock strength. Heated walls (red circles), cooled walls (blue triangles), and high-Re cooled wall (cyan square).

In contrast, Grossman and Bruce [20] found values ranging from 3.37 to 5.07, while Matheis and Hickel [21] found $\mathcal{P}_s = 1.6$ for regular and irregular SBLI at different deflection angles. In a much earlier study, Erdos and Pallone [15] proposed the specific value $\mathcal{P}_s = 4.22$ for turbulent flow (and $\mathcal{P}_s = 0.81$ for laminar flow). Clearly the free interaction scaled pressure at separation does not seem to have a universal value.

In what is presumably a coincidence, the Erdos and Pallone [15] value of $\mathcal{P}_s = 4.22$ instead corresponds very closely to where the similarity between the different cases breaks down in the present study.

Erdos and Pallone [15] also proposed that $\mathcal{P}_p$, the value at the pressure plateau, should be 6.0 in a turbulent flow and 1.47 in a laminar flow. Matheis and Hickel [21] found $\mathcal{P}_p = 7.4$ in their study, which agrees well with the present cases that display a strong interaction.

3.4 Interaction length scaling

The interaction length L_{int} is defined as the distance between the foot of the separation shock and the extrapolated wall impact point of the incident shock. In this study, the interaction length is well approximated by $L_{int} = x_{imp} - x_{sep}$. Note that the separation location has the same behavior as the interaction length and that the reattachment position remains constant for weak interactions and changes only for strong ones [1].

Using mass conservation properties along the interaction, Souverein *et al.* [22] carried out a scaling analysis, where the interaction length L_{int} was normalized by the displacement thickness of the incoming boundary layer δ_0^* and the function $g_3(\beta, \varphi) = \sin(\beta - \varphi)/[\sin(\beta)\sin(\varphi)]$ that takes into account the imposed flow deflection and the Mach number (φ and β are the deflection and shock angles, respectively). They then argued that this normalized interaction length should depend on a separation criterion defined as $\Delta P/\Delta P_{sep}$, where ΔP is the pressure jump across the interaction and ΔP_{sep} is the pressure jump required to make the boundary layer separate. The latter was estimated as $\Delta P_{sep} \approx q_0/k_1$, where q_0 is the dynamic pressure in the incoming boundary layer and k_1 is a coefficient for which they recommended the values of 3 for low Reynolds numbers ($Re_\theta \approx 5 \times 10^3$) and 2.5 for higher Reynolds numbers ($1 \times 10^4 < Re_\theta < 3 \times 10^5$). The interaction length scaled according to this scaling is shown in Fig. 11(a) together with a compilation of data found in the

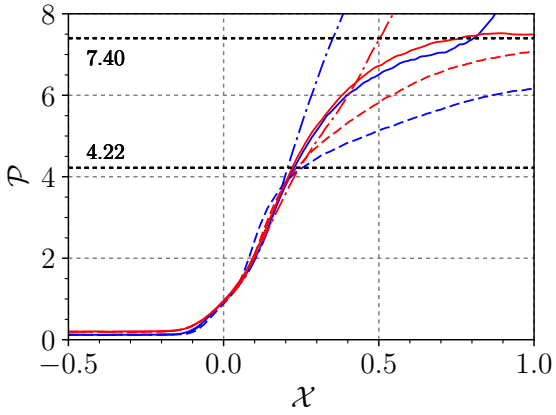

Figure 10: Similarity function $\mathcal{P}$ (scaled pressure; Eq. 3) plotted versus $\mathcal{X}$ (distance from separation point; Eq. 4) evaluated for all SBLI cases. Cases: SBLI-0.8-06 (blue dashed), SBLI-0.8-10 (blue dash-dotted), SBLI-0.8-14 (blue solid), SBLI-1.9-06 (red dashed), SBLI-1.9-10 (red dash-dotted), SBLI-1.9-14 (red solid).

literature. This scaling works well for weak interactions but shows a larger spread between heated and cooled walls for stronger interactions.

Jaunet *et al.* [5] modified the scaling relationship through use of the free interaction theory by Chapman *et al.* [14] to better account for the effects of wall temperature. Specifically, they adjusted the estimation of the pressure jump required to make the boundary layer separate to $\Delta P'_{sep} = k_2 q_0 \sqrt{2C_{f0}/(M_0^2-1)^{1/2}}$, which now explicitly depends on the friction coefficient and the Mach number of the incoming boundary layer. They computed the value of the k_2 coefficient as $k_2 = 7.14$ based on an adiabatic case at $M_\infty = 2.28$, and validated the scaling on a range of cases at that Mach number but with different wall temperatures; this scaling was also found to be very accurate at the same $M_\infty = 2.28$ for heated/adiabatic/cooled walls and different Reynolds numbers in the Mach 2.3 DNS.

The Jaunet *et al.* [5] scaling is validated for the present $M_\infty = 5$ in Fig. 11(b) together with the experimental data from [5]. The higher Mach number cases do not collapse on the lower Mach number ones. Adjusting the coefficient to $k_2 = 15$ produces a much better agreement across the Mach numbers, which shows that this coefficient is not a "constant"; it depends at least on the Mach number. We note that the dependence on the interaction strength (or separation criterion) agrees well after adjusting the k_2 coefficient, which shows that the Jaunet *et al.* [5] scaling does capture the correct dependence on ΔP and T_w/T_r.

4 Mean velocity scaling

The mean velocity profile in compressible boundary layers does not follow the log-law due to the density and viscosity variations caused by the viscous heating. The classic way to deal with this is to use the Van Driest (1951) [28] "transformation", and to then assume that the "transformed" (or "scaled") mean velocity profile should agree with the log-law. This velocity scaling is used in empirical friction formulas, wall-models for LES, and is often used to calibrate RANS models.

The Van Driest transformation is known to be accurate for adiabatic walls at all Mach numbers, but has also been known to be inaccurate for strongly non-adiabatic walls. In prior work [29],

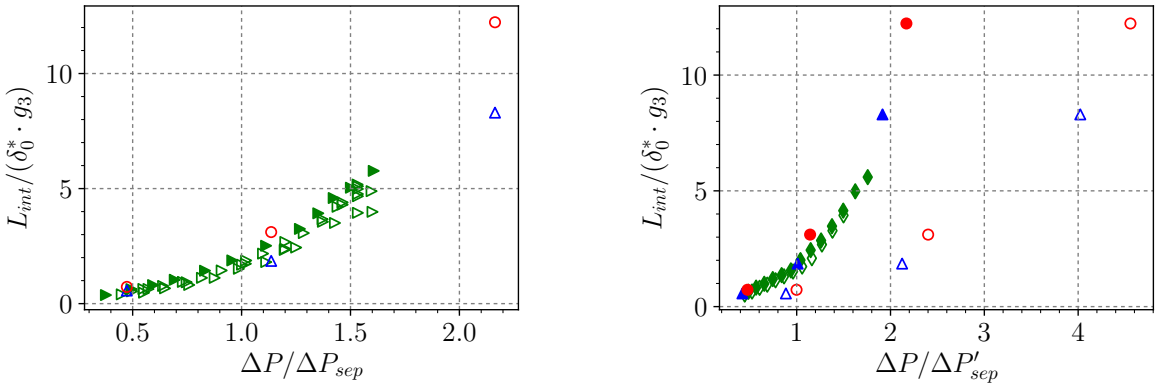

Figure 11: Normalized interaction length L_{int} as a function of the separation criteria by Souverein *et al.* [22] (left) and Jaunet *et al.* [5] (right). DNS with cooled (blue triangles) and heated (red circles) wall; open symbols scaled using the original constants ($k_1 = 3$ in the left figure, $k_2 = 7.14$ in the right), filled symbols scaled using the modified constant $k_2 = 15$. The compilation of results discussed in Souverein *et al.* [22] is also reported: adiabatic walls (green open triangles) [23, 24, 25, 26] and heated walls (green filled triangles) [27]. Experimental data from Jaunet *et al.* [5] at Mach ($M_\infty = 2.3$) and Reynolds ($Re_\theta = 5 \times 10^3$) numbers are also reported: adiabatic walls (green open diamonds) and heated walls (green filled diamonds).

we introduced a different scaling or transformation, and tested it on channel flows with excellent results – see Fig. 12(a). When applying this scaling theory to external boundary layers, we (and other research groups) reached two conclusions: (i) the theory accurately handles different T_w/T_r conditions even in boundary layers (so it does account for the non-adiabatic nature of the wall); and (ii) surprisingly, there was a small offset from the log-law that did not appear in channel flows (compare Figs. 12(a) and 12(b)).

The second conclusion was surprising, since the theory seemed equally valid for both internal and external flows (no specific assumption either way was made). During the final year of the project we thus started investigating this in more depth. When applying the scaling to higher Mach numbers (Fig. 12(c)), the offset from the log-law grew larger, something which was totally unexpected.

The only conclusion is that there is something missing from the theory. The Trettel & Larsson theory does account for non-adiabatic effects much more accurately than the classic Van Driest theory, at least up to Mach 3. On the other hand, the Van Driest theory accounts for Mach number variations more accurately, at least above Mach 3 or so. Therefore, neither theory is entirely correct, and one should be able to develop a new scaling theory that surpasses both. This is very important from a fundamental perspective but also from a pragmatic one: the assumed scaling (with Mach number and wall temperature) is at the core of friction formulae (e.g., VD-II), wall-models for LES, etc.

We started working on developing a new mean velocity scaling theory during the last year of the project. At this point we have found a "transformation" that works better than existing ones, but which has no real physical justification; the "transformation" was simply arrived at through calibration against DNS data. While perhaps practically useful, this is not really advancing the scientific state-of-the-art. We will continue working on this issue during the coming years.

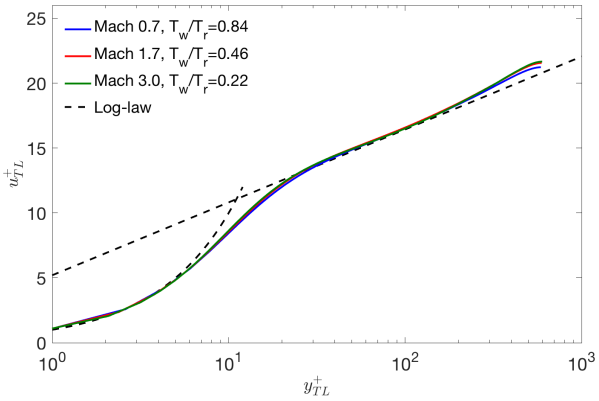

(a) Channel flows, from Trettel & Larsson (2016) [29].

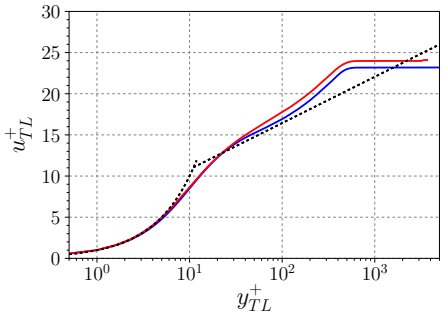

(b) Mach 2.3 boundary layer, at $T_w/T_r = 1.0$ (blue) and $T_w/T_r = 1.9$ (red), from current work.

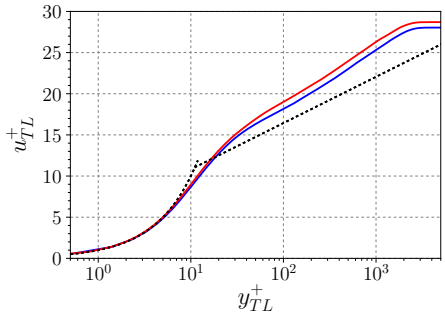

(c) Mach 5.0 boundary layer, at $T_w/T_r = 0.8$ (blue) and $T_w/T_r = 1.9$ (red), from current work.

Figure 12: Mean velocity profiles scaled using the Trettel & Larsson (2016) [29] theory.

References

[1] P. S. Volpiani, M. Bernardini, J. Larsson, Effects of a nonadiabatic wall on supersonic shock/boundary-layer interactions, Phys. Rev. Fluids 3 (2018) 083401.

[2] P. S. Volpiani, A. Wagner, M. Bernardini, J. Larsson, Using large-eddy simulations to design a new hypersonic shock/boundary-layer interaction experiment, in: AIAA Scitech 2019 Forum, 2019, p. 0098.

[3] E. Schülein, Skin friction and heat flux measurements in shock/boundary layer interaction flows, AIAA J. 44 (8) (2006) 1732–1741.

[4] P. S. Volpiani, M. Bernardini, J. Larsson, Effects of a nonadiabatic wall on hypersonic shock/boundary-layer interactions, under review for Phys. Rev. Fluids.

[5] V. Jaunet, J. F. Debiève, P. Dupont, Length scales and time scales of a heated shock-wave/boundary-layer interaction, AIAA J. 52 (11) (2014) 2524–2532.

[6] J. Délery, J.-P. Dussauge, Some physical aspects of shock wave/boundary layer interactions, Shock waves 19 (6) (2009) 453–468.

[7] P. Bruce, D. Burton, N. Titchener, H. Babinsky, Corner effect and separation in transonic channel flows, J. Fluid Mech. 679 (2011) 247–262.

[8] E. E. Zukoski, Turbulent boundary-layer separation in front of a forward-facing step., AIAA J. 5 (10) (1967) 1746–1753.

[9] M. Bernardini, I. Asproulias, J. Larsson, S. Pirozzoli, F. Grasso, Heat transfer and wall temperature effects in shock wave turbulent boundary layer interactions, Phys. Rev. Fluids 1 (8) (2016) 084403.

[10] V. Pasquariello, S. Hickel, N. A. Adams, Unsteady effects of strong shock-wave/boundary-layer interaction at high reynolds number, J. Fluid Mech. 823 (2017) 617–657.

[11] L. H. Back, R. F. Cuffel, Changes in heat transfer from turbulent boundary layers interacting with shock waves and expansion waves, AIAA J. 8 (10) (1970) 1871–1873.

[12] M. Holden, Shock wave-turbulent boundary layer interaction in hypersonic flow, in: 15th Aerospace Sciences Meeting, 1977, p. 45.

[13] F. Hung, D. Barnett, Shockwave-boundary layer interference heating analysis, in: 11th Aerospace Sciences Meeting, 1973, p. 237.

[14] D. Chapman, D. Kuehn, H. Larson, Investigation of separated flows in supersonic and subsonic streams with emphasis on the effect of transition, Tech. Rep. TN-3869, National Advisory Committee for Aeronautics (1958).

[15] J. Erdos, A. Pallone, Shock-boundary layer interaction and flow separation, Heat Transfer and Fluid Mechanics Institute Procs.

[16] P. Carrière, M. Sirieix, J.-L. Solignac, Similarity properties of the laminar or turbulent separation phenomena in a non-uniform supersonic flow, in: Applied mechanics, Springer, 1969, pp. 145–157.

[17] A. F. Charwat, Supersonic flows with imbedded separated regions, in: Advances in Heat Transfer, Vol. 6, Elsevier, 1970, pp. 1–132.

[18] J. Délery, J. G. Marvin, Shock-wave boundary layer interactions, Tech. Rep. AGARD-AG-280, Advisory Group for Aerospace Research and Development (1986).

[19] H. Babinsky, J. K. Harvey, Shock wave-boundary-layer interactions, Vol. 32, Cambridge University Press, 2011.

[20] I. J. Grossman, P. J. K. Bruce, Confinement effects on regular–irregular transition in shock-wave–boundary-layer interactions, J. Fluid Mech. 853 (2018) 171–204.

[21] J. Matheis, S. Hickel, On the transition between regular and irregular shock patterns of shock-wave/boundary-layer interactions, J. Fluid Mech. 776 (2015) 200–234.

[22] L. J. Souverein, P. G. Bakker, P. Dupont, A scaling analysis for turbulent shock-wave/boundary-layer interactions, J. Fluid Mech. 714 (2013) 505–535.

[23] P. Dupont, C. Haddad, J. F. Debieve, Space and time organization in a shock-induced separated boundary layer, J. Fluid Mech. 559 (2006) 255–277.

[24] S. Piponniau, J. P. Dussauge, J. F. Debieve, P. Dupont, A simple model for low-frequency unsteadiness in shock-induced separation, J. Fluid Mech. 629 (2009) 87–108.

[25] L. J. Souverein, B. W. V. Oudheusden, F. Scarano, P. Dupont, Application of a dual-plane particle image velocimetry (dual-piv) technique for the unsteadiness characterization of a shock wave turbulent boundary layer interaction, Measurement Science and Technology 20 (7) (2009) 074003.

[26] L. J. Souverein, P. Dupont, J.-F. Debiève, B. W. V. Oudheusden, F. Scarano, Effect of interaction strength on unsteadiness in shock-wave-induced separations, AIAA J. 48 (7) (2010) 1480–1493.

[27] H. Laurent, Turbulence d'une interaction onde de choc/ couche limite sur une paroi plane adiabatique ou chauffée, Ph.D. thesis, Université d'Aix-Marseille II, Marseille, France (1996).

[28] E. R. Van Driest, Turbulent boundary layer in compressible fluids, J. Aero. Sci. 18 (3) (1951) 145–160.

[29] A. Trettel, J. Larsson, Mean velocity scaling for compressible wall turbulence with heat transfer, Phys. Fluids 28 (2) (2016) 026102.